

# Measuring THz Repetition Rate of Microresonator Optical Frequency Combs using Electro-Optic Modulation

**Emilio Pérez de Juan**  
Undergraduate Honor Thesis



Department of Physics and Astronomy  
University of New Mexico  
Albuquerque, NM 87106, USA

# TABLE OF CONTENT

I. Introduction	
A. Background of Frequency Combs	pg[2-3]
B. Importance of Frequency Comb Generation and microcombs	pg[3-5]
C. Motivation for Research and Thesis Content	pg[6]
II. Theory	
A. Principles of Electro-Optic Modulation	pg[7-8]
B. Key Parameters and Characteristics	pg[8-11]
III. Experimental Set-up	
A. Description of the Experimental Configuration	pg[12-14]
B. Calibration and Control Procedures	pg[14-15]
IV. Results	
A. Measured EOM microcomb	pg[16-17]
B. Suggestions for Further Research and Development	pg[17-18]
C. Conclusion	pg[18]
V. Acknowledgements	pg[18]
VI. Bibliography	pg[19]

## 1. INTRODUCTION

### A. Background of Frequency Combs

Precision control of optical frequency is critical for numerous disciplines in modern scientific research, from telecommunications to spectroscopy, and from fundamental physics to photonics and quantum optics. One of the important developments in this field is the optical frequency comb (OFC). This thesis will explore the importance of understanding the limits of frequency combs in creating and measuring highly precise and tunable frequency sources.

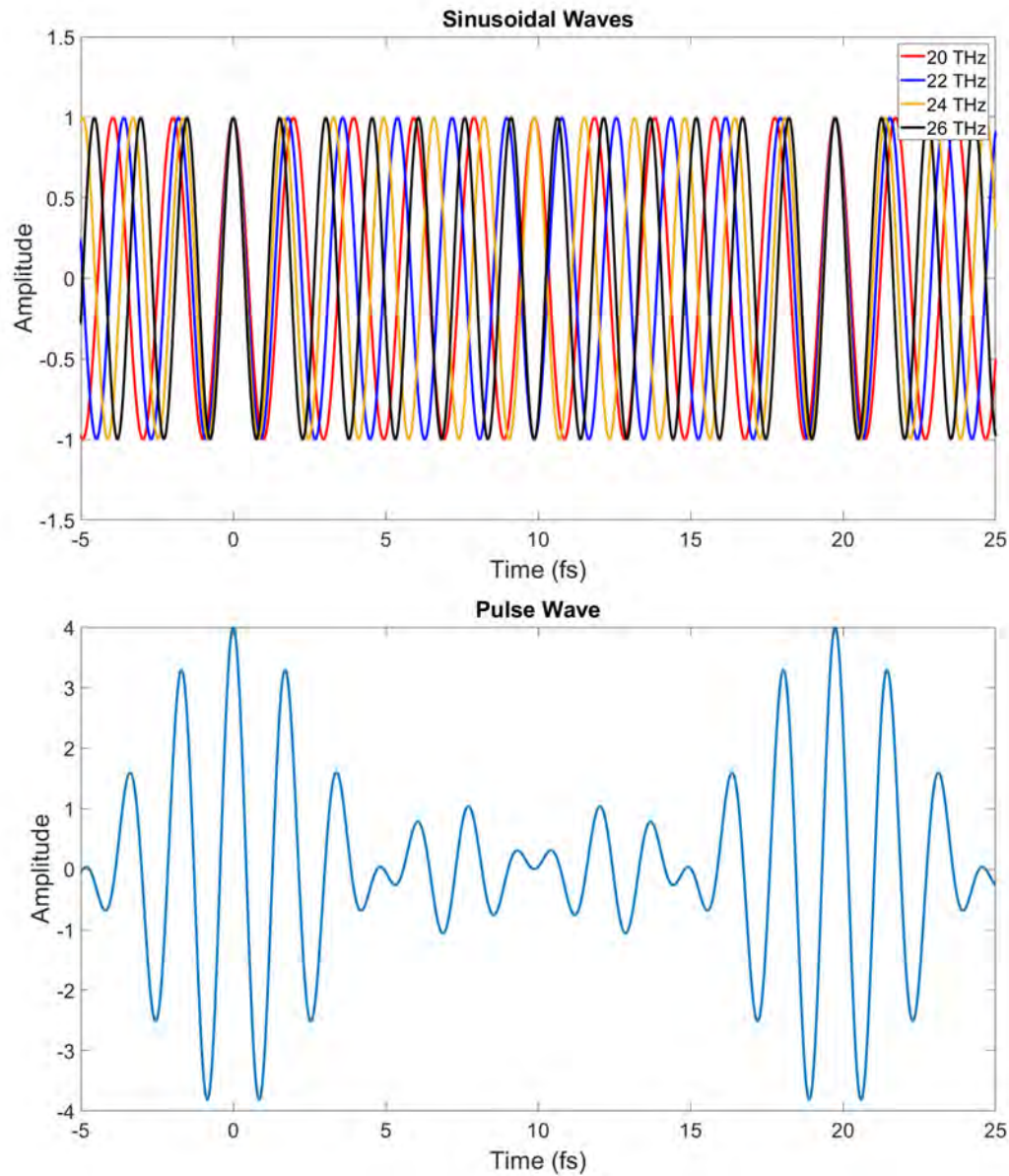


FIG. 1: The top image illustrates sinusoidal waves of various frequencies and equal phase, spread by a constant frequency difference, where constructive and destructive interference patterns are observable. In the bottom image, the waves from the top are combined. The maximum amplitude of this waveform occurs when total constructive interference is present, while it reaches its minimum during destructive interference. This waveform's shape is delineated by the carrier and envelope of the wave. Due to their similar frequency differences and in-phase alignment, this waveform emerges, known as a pulse train, with repetitions delimited by a fixed period determined by that frequency difference, referred to as the frequency of repetition.

The optical frequency comb can be understood as a basic summation of plane waves of light. In figure 1, we see a set of waves with different yet similar frequencies. When many of these frequencies are combined, the resulting carrier wave forms a train of distinct pulses. The oscillating signal obtained in this wave contains all of the frequencies in figure 1 and they are limited by the envelope (which outlines the outer limits of the wave, amplitude and shape) and the frequency of the signal, the carrier (which is a fixed frequency determined by the light source, such as the laser's lasing frequency). In frequency comb generation, the combination of many frequencies creates a series of pulses temporally spaced by the inverse of the frequency of repetition of the pulse train  $f_{rep}$ , in our case we use optical frequencies.

Optical frequency combs are optical waveforms whose spectra consist of a series of discrete, phase-matched, and equally spaced frequency lines (representing various colors of light), as depicted in figure 2. There are two methods of analyzing such a signal: one involves examining the signal in the time domain, where the pulse train resulting from the combination of many waves and the elongated time between waveform repetitions can be observed; the other entails examining the signal in the frequency domain, where Fourier analysis reveals the different frequencies comprising the wave. Optical frequency combs are often referred to as "optical rulers" due to their composition of fixed and evenly spaced frequencies of light in multiples of  $f_{rep}$  (along with a common offset). Therefore, since  $f_{rep}$  remains constant over the pulse lifetime, we often call this also as "ruler of time".

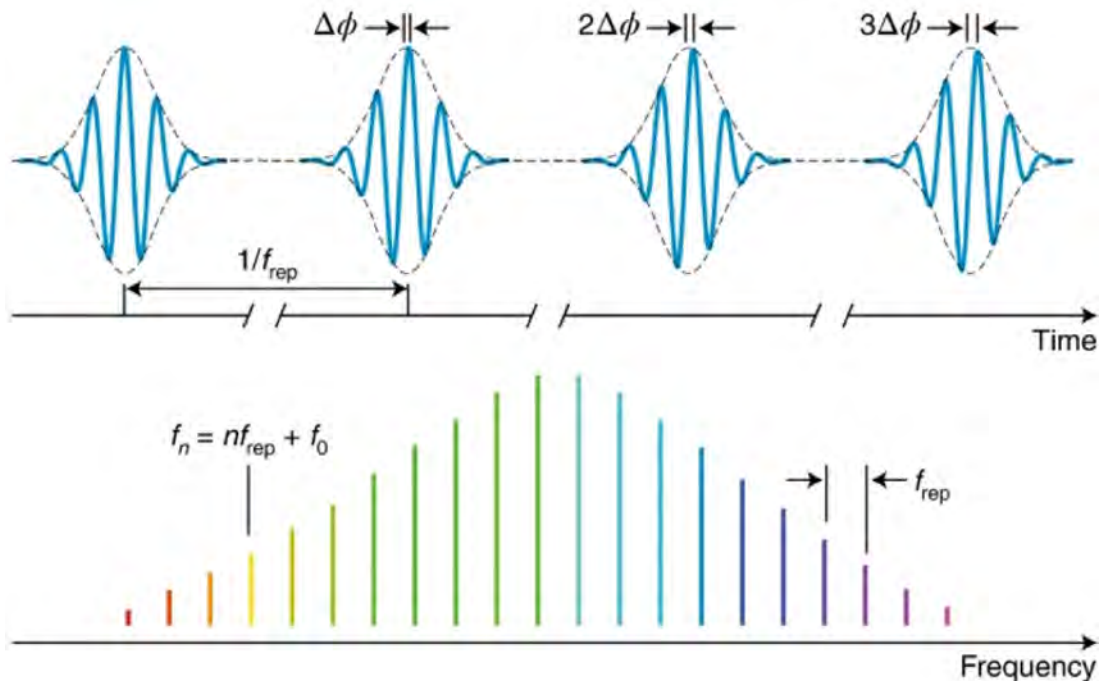


FIG. 2: This image presents an illustration of an optical frequency comb. The upper image represents an example in the time domain, where the pulse waveform repeats in time with a frequency of  $f_{rep}$ . The lower image depicts the frequency domain, wherein all frequencies are displayed as lines via Fourier analysis, evenly spaced by  $f_{rep}$ . The parameter  $f_0$  denotes the carrier-envelope offset, the study of which extends beyond the scope of this research. Reproduced from [1].

## B. Importance of Frequency Comb Generation and microcombs

Frequency combs are generated through a phenomenon known as four-wave mixing (FWM), a nonlinear effect wherein photons of differing or similar energies interact in a medium, resulting in the creation of a new photon pair with altered energies (while energy conservation is maintained), as shown in figure 3. In our laboratory, we employ continuous pumping of a laser with a constant frequency, which, depending on the experiment, may be either  $1.5 \mu\text{m}$  or  $1 \mu\text{m}$ .

There are two types of FWM: degenerate and non-degenerate. Both operate similarly, with degenerate FWM

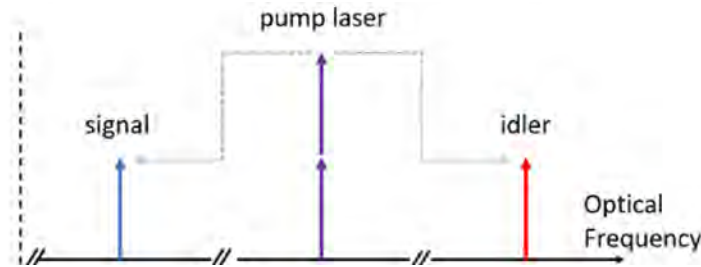


FIG. 3: . The primary pump, comprising photons of equal energy, consistently generates two distinct photons through FWM: the carrier and the signal. These terms are commonly utilized in the context of telecommunications, where the signal photon possesses greater energy than the idler photon, which has the lowest energy among the generated photons.

involving two original photons of equal energy, while non-degenerate FWM involves two photons with differing energies. Despite this distinction, both types yield a similar outcome, producing one photon with higher energy and another with lower energy, as depicted in figure 4. In our context, achieving FWM requires surpassing a threshold power level. When multiple instances of FWM occur sequentially, it is referred as "cascade FWM," ultimately resulting in the generation of an optical frequency comb.

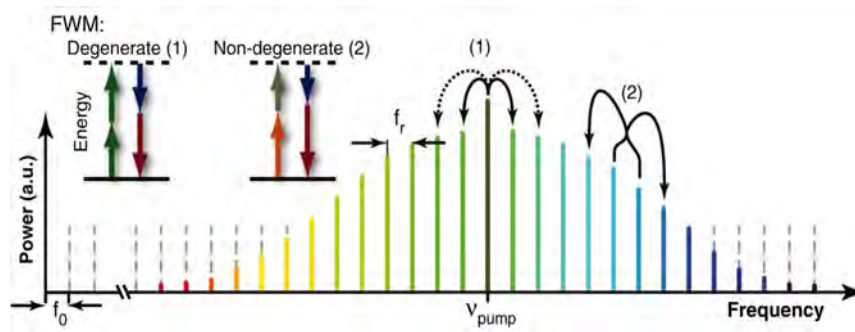


FIG. 4: . In FWM cascade processes, photons from the main pump undergo multiple annihilation events with one another, generating an optical frequency comb. These annihilation events can occur between photons of different energies, either in degenerate or non-degenerate configurations. Regardless of the specific type, this cascade process leads to the formation of the optical frequency comb. Reproduced from [2].

In our laboratory, we produce optical frequency combs by exploiting the Kerr effect within optical microresonators, commonly referred to as "microcombs." These microcombs are compact devices ranging from millimeter to micrometer scales. They confine light in their structures (as illustrated in figure 5) through total internal reflection. Available in various geometries such as ring, toroidal, and rod shapes, as well as differing sizes and materials, these microresonators offer versatile options for experimentation. It is notable that some geometries do not rely on total internal reflection, although they are also employed in this context. We have selected the ring microresonator configuration due to its advantages. Firstly, it enables rapid and straightforward integration onto chips, akin to integrated circuits. Secondly, its compatibility with fiber optics streamlines experimental setups, enhancing overall efficiency and versatility.

In our laboratory, we utilize microresonator rings to confine a single-frequency pump laser within a small volume, thereby generating high light intensities necessary for nonlinear optical processes. As depicted in figure 6, we employ a standard setup for optical frequency comb generation. A continuous tunable continuous-wave (CW) laser serves as the pump source, emitting light at a fixed frequency. This light is amplified to surpass a power threshold required to initiate the FWM process. Subsequently, as illustrated in figure 7, the light is coupled into the resonator, where FWM occurs. The resulting waveform can then be analyzed using an oscilloscope to observe the signal of the wave.

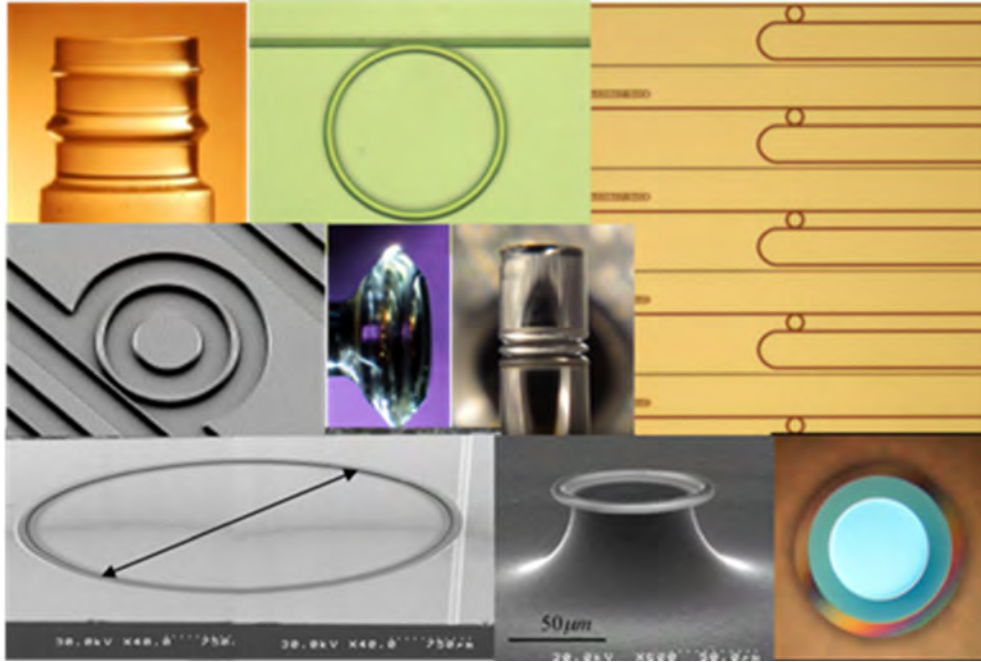


FIG. 5: . Various microresonator materials and geometries, ranging from toroidal, ring, disk, whispering-gallery-mode, microsphere, etc. Reproduced from [3]-[11] .

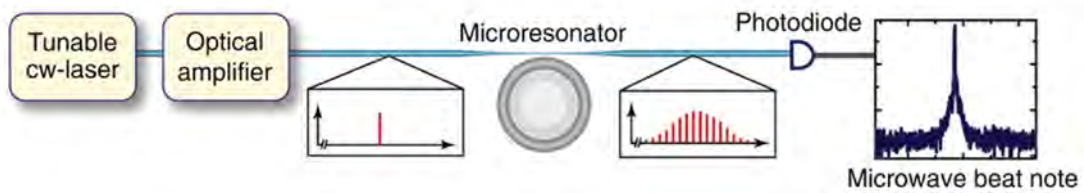


FIG. 6: . In an optical frequency comb creation setup, a main pump source, typically a fixed continuous-wave laser, undergoes amplification to exceed the threshold necessary for four-wave mixing to initiate. Subsequently, within the resonator, the optical frequency comb is generated. Later, the resulting signal can be detected using a photodiode. In this particular case, the experiment involved working with microwave frequencies. Reproduced from [2]

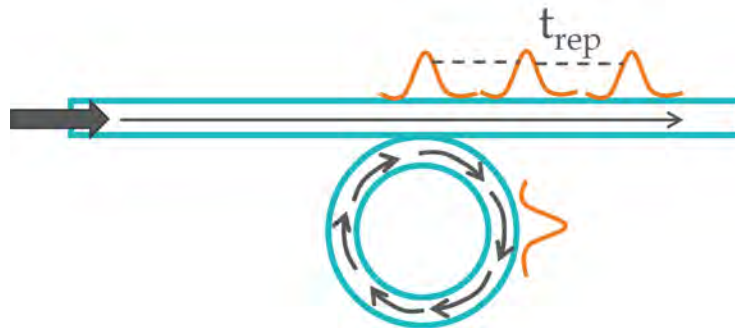


FIG. 7: . The diagram depicts the pathway of light as it enters the resonator, adheres to its geometric configuration, undergoes FWM within the resonance, and exits the resonator carrying the optical frequency comb. The repetition rate of the comb structure is determined by the time period of repetition, denoted as  $t_{rep}$ , which is associated with the repetition frequency  $f_{rep}$ .

### C. Motivation for Research and Thesis Content

This research aims to investigate the frequency of repetition ( $f_{rep}$ ) of one of our microcombs in order to study the operational limits and behaviors of these devices in creating optical frequency combs, particularly solitons. Solitons, or solitary waves (seen in figure 8), are low noise frequency combs with a stable waveform that sustain their shape over time indefinitely, which exist at specific conditions in the resonator.

The existence of solitons arises from a balance between nonlinearity within the material, which tends to disperse wave packets, and dispersion, which can counteract dispersion by inducing self-focusing effects [12]. Direct measurement of  $f_{rep}$  facilitates the validation of our prevailing understanding of comb creation processes. The overarching objective of this research is to enhance comprehension of our devices' limitations, thereby improving the generation of optical frequency combs and solitons. We opted to utilize  $1\ \mu\text{m}$  laser microcombs instead of  $1.5\ \mu\text{m}$  to leverage self-focusing during microcomb creation. In an optical fiber, the intrinsic waveguide forms guided modes. The increased frequency correlates with heightened self-focusing, thereby amplifying nonlinear effects within the combs. This, in turn, significantly reduces the area of each mode and aids in mitigating the nonlinear Kerr effect generated within the resonator.

For the primary objective of this investigation, our aim is to measure the  $f_{rep}$  of one of our  $\text{Si}_3\text{N}_4$  devices. Modes for  $1\ \mu\text{m}$  light typically disperse by approximately 1 THz. Utilizing an Electro-Optic Modulator (EOM), we will generate multiple sidebands separated by roughly 18 GHz of  $f_m$  (modulation frequency), which are readily measurable using conventional devices. This is imperative as the THz range poses challenges for measurement, given that devices often lack sufficient resolution for higher frequencies. Here, we present the comprehensive setup comprising essential apparatus assisting in the development of the EOM setup, alongside various calibrations and configurations necessary for complete modulation. The use of EOM, will allow us to generate diverse sidebands from a main pump in a range measurable (GHz) for conventional devices since 1 THz of spanning is hard to be measure from an Optical Spectrum Analyzer, completing in that way the spanning of the  $f_{rep}$  of our OFCs.

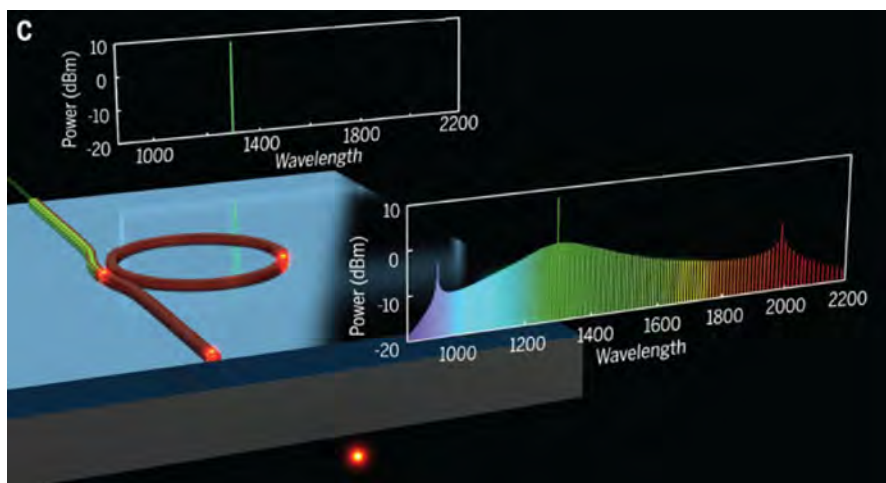


FIG. 8: . The illustration portrays a soliton generated within a microring resonator. The geometry of the device, along with its material composition, dictates the waveform obtained, and these parameters are intentionally designed to facilitate soliton formation. The microring resonator's structure confines light within a closed-loop configuration, promoting strong light-matter interactions. The material properties of the resonator, such as its refractive index and dispersion characteristics, play a crucial role in shaping the soliton waveform. The intentional design of the microring resonator ensures that the generated soliton exhibits desired characteristics, such as stability, low noise, and the ability to maintain its shape over extended periods. Reproduced from [12].

## 2. THEORY

### A.Principles of Electro-Optic Modulation

Electro-optic modulation (EOM) is a fundamental technique in optics employed to manipulate the characteristics of light, including its phase, intensity, polarization, or frequency, utilizing an external electric field (figure 9 shows an Electro-optic modulator). This modulation mechanism is accomplished through the linear electro-optic effect, also known as the Pockels effect, wherein the refractive index ( $n$ ) of a material undergoes alteration in response to an applied electric field ( $E$ ). This phenomenon can be mathematically described by the following equation:

$$n(E) = n_0 + a_1 E + \frac{1}{2} a_2 E^2 + \dots \quad (1)$$

Where  $a_1$  relates to the  $\chi_1$  linear electro-optic coefficient of the Pockels effect and  $a_2$  to the  $\chi_2$  nonlinear quadratic electro-optic effect, which refers to the Kerr effect.

The linear electro-optic effect emerges from the interaction between an electric field and the optical characteristics of specific materials, termed electro-optic materials. Only non-centrosymmetric materials demonstrate a variation in refractive index when subjected to an electric field, typically possessing a crystalline structure. Examples of such materials include Lithium Niobate ( $\text{LiNbO}_3$ ), Lithium Tantalate ( $\text{LiTaO}_3$ ), Potassium Titanyl Phosphate (KTP), among others. Furthermore, certain materials exhibit a quadratic or nonlinear electro-optic effect, wherein the change in refractive index is proportional to the square of the electric field. These materials are often employed in the creation of OFCs and other nonlinear optical devices[13].

Electro-optic modulation finds broad application across diverse fields, including telecommunications, optical signal processing, laser technology, and optical sensing. Its versatility and effectiveness in controlling light properties make it a valuable tool in modern optical systems and applications.

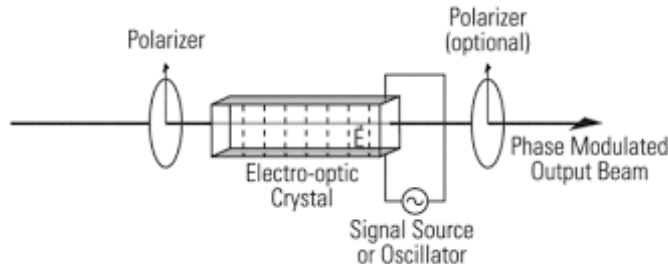


FIG. 9: . An Electro-Optic Modulator is used to modulate the intensity or phase of a laser beam. It typically consists of an electro-optic crystal, some polarizers, and a signal source. The electro-optic crystal is the core component of the EOM. It's a material that exhibits the electro-optic effect, meaning its optical properties change in response to an applied electric field.

The polarizers are used to control the polarization of the incoming laser beam. It ensures that only light with a specific polarization orientation passes through. The signal source provides the electrical signal that drives the EOM. This signal determines how the optical properties of the crystal change, consequently modulating the laser beam. Reproduced from [14].

There are different ways in how an EOM can modulate a signal. They leverage the linear electro-optic effect to manipulate light and its polarization, offering distinct advantages over conventional mechanical devices, particularly in handling higher frequencies with remarkable speed, often in the GHz range. These modulators typically consist of an array of Pockels cells, where light propagates through a crystal and accumulates phase delays controlled by varying electric voltages.

In our setup, the EOM features a crystal like lithium niobate. By applying a variable electric voltage, called the half-wave driving voltage ( $V_\pi$ ), the refractive index changes, inducing a phase shift in the incident light beam. This modulation occurs at a fixed frequency ( $f_m$ ), effectively altering the signal's frequency by that amount.

A key application of such phase modulation, related to our lab's objectives, involves generating sidebands from a monochromatic laser beam. By applying a varying potential voltage at a specific frequency and small amplitude, sidebands emerge, with their amplitudes diminishing as they move away from the original monochromatic input. This process enables the creation of spectral components around the central frequency, facilitating the application to divide THz of range into GHz.

In the EOM applying a voltage of  $V_\pi$  induced a phase shift of  $\pi$  radians. This voltage level is significant because it enables achieving full modulation from  $-V_\pi$  to  $+V_\pi$  essentially completing a loop in the phase shift cycle. Typically,  $V_\pi$  for EOMs ranges in the hundreds to thousands of volts. Such high voltages necessitate the use of an amplifier to ensure effective operation. The phase caused by the EOM affects the emergent electric field as shown in Eqn. 2.

$$E = E_0 \sin(2\pi f_0 t + \Phi_0(\sin(2\pi f_m t))). \quad (2)$$

where  $E_0$  is the initial amplitude of the incoming electric field,  $f_0$  it's original frequency and  $\Phi_0$  is the phase amplitude of the modulation. This change in the electric field is related to the amplitude of the peak-to-peak driving voltage ( $V_{PP}$ ) of the modulator where this voltage is required to achieve a full modulation depth ( $2V_\pi = V_{PP}$ ), it can be expressed as in Eqn. 3.

$$\frac{\varphi_0}{\pi} = \frac{V_{PP}}{2V_\pi}. \quad (3)$$

where  $\varphi_0$  is the phase modulation depth. Controlling the half-wave driving voltage not only influences the phase shift but also affects the power distribution of the sidebands. This aspect is particularly significant for our research objectives. However, RF sources commonly specify their performance in terms of power (dBm) rather than voltage. Therefore, we need to convert the desired voltage levels into corresponding power levels to accurately characterize the requirements for the amplifier. To achieve full modulation depth and ensure the generation of all necessary sidebands for our microcomb optical experiment, we must determine the relative power levels needed from the amplifier. This means converting the voltage levels required for modulation ( $V_\pi$ ) into corresponding power levels. The conversion from voltage to power involves several factors, including the impedance  $Z$  of the system and the efficiency of the amplifier. By considering these factors and employing appropriate conversion formulas, we can establish the relationship between the desired voltage levels for modulation and the corresponding power levels required from the amplifier. Eqn 4. portrays this conversion:

$$P_{mW} = \frac{1000mW}{1W} \frac{(V_{rms})^2}{Z}. \quad (4)$$

where  $V_{rms}$  is the root mean square when the driving voltage is sinusoidal.

## B.Key Parameters and Characteristics

**Sidebands:** Understanding  $V_{PP}$  is crucial for our objective of creating the necessary sidebands to span the complete 1 THz range. While  $V_\pi$  represents a fixed property of the modulator itself (in our case, 3.91 V),  $V_{PP}$  pertains to the variation of the electrical field over time, directly influencing the modulation depth achievable. In our context, the modulation phase, as depicted in figure 10 and governed by Eqn. 3, solely relies on  $V_{PP}$  since  $V_\pi$  remains constant. Therefore, the modulation phase is expressed in terms of  $V_\pi$ , emphasizing the importance of  $V_{PP}$  in determining the modulation depth required for creating a sufficient number of sidebands. Table 1 provides the measured required modulation depth obtained from simulations to determine the  $V_{PP}$  necessary for generating different numbers of sidebands consistently, and hence, use them in the modulation for the correct spanning.

TABLE I: The table illustrates that an increase in  $V_{PP}$  results in a corresponding augmentation of the modulation phase, consequently facilitating the generation of a greater number of sidebands. The third term denotes the conversion from modulation depth in terms of  $V_\pi$  to power in dBm, accomplished through the transformation of mW, as described in Equation 4, into dBm. Reproduced from MATLAB simulation Thorlabs webpage [15] of figure 10.

$N^{th}$ of sidebands	Modulation depth	RF power (dBm)
1	0.58	10.84
2	1	15.58
4	1.72	20.29
12	4.42	28.48
16	6.82	32.25

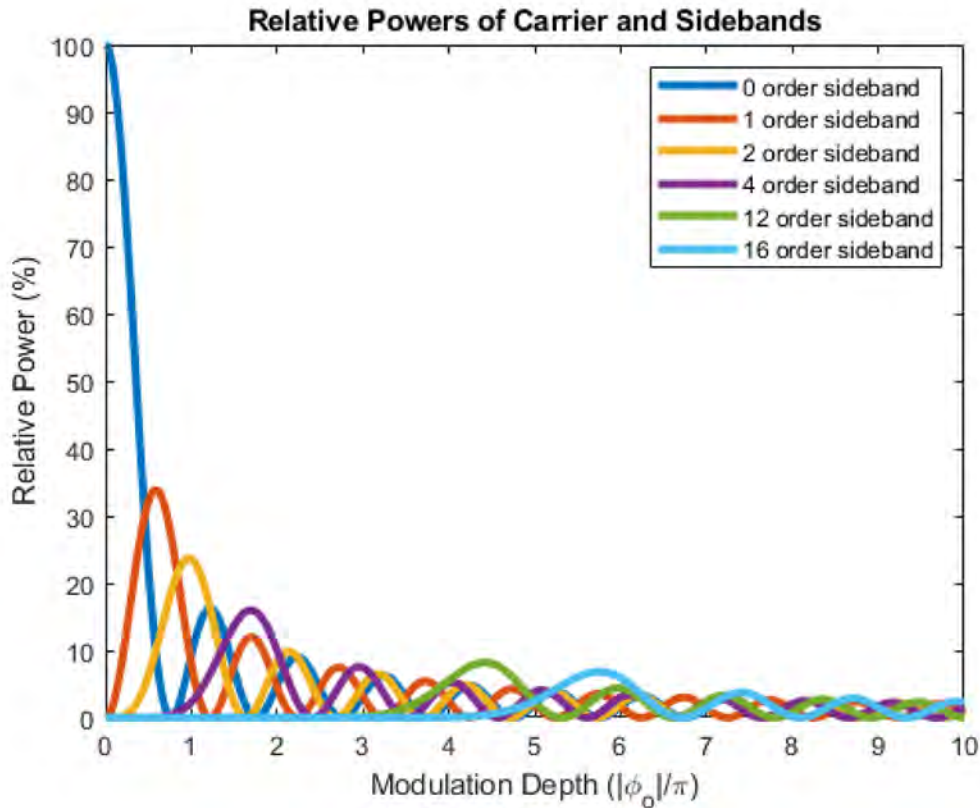


FIG. 10: MATLAB simulation from the Thorlabs webpage [15]. The simulation shows the required modulation phase and the relative power for each of the created sidebands. Specifically  $V_{PP}$  needs to be resolved to create a fix amount of sidebands, modulating in this case at 18 GHz. The objective is to generate 16 sidebands on either side of each comb mode, thereby spanning a total bandwidth of 1 THz.

The key aspect in this research is to generate a sufficient number of sidebands spanning the 1 THz separation between adjacent modes within an optical frequency comb. To achieve this, we will select two modes from our optical frequency comb, as depicted in figure 11, from which sidebands will be generated in both the right and left directions, as illustrated in figure 12.

In our experimental setup, we will modulate the signal at intervals of 18 GHz between adjacent modes until we cover half of the desired 1 THz span from each mode. While it is conceivable to utilize a single branch of modulation to achieve the entire 1 THz span, this approach necessitates a significant amount of power beyond the capabilities of our devices. Therefore, we will employ both branches of modulation—left and right—simultaneously. It's important to note that controlling the direction of modulation is not feasible in this setup. Sidebands generated from a phase modulator will manifest in every possible direction across the frequency spectrum ( $f_0 \pm n f_m$ ), ensuring comprehensive coverage of the desired frequency span.

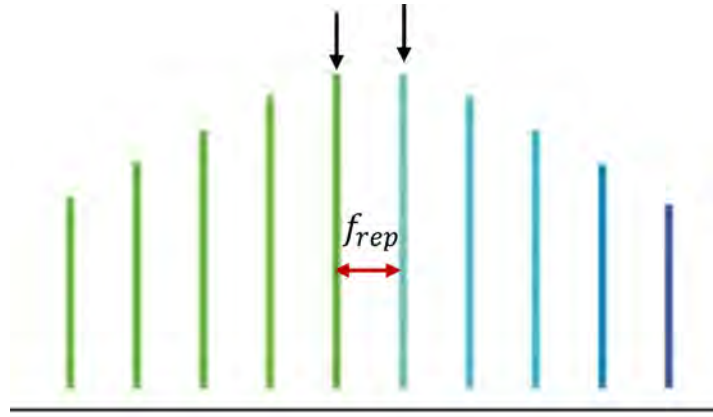


FIG. 11: An illustration of two closely spaced modes, which will serve as the basis for our Electro-Optic Modulator experiment.

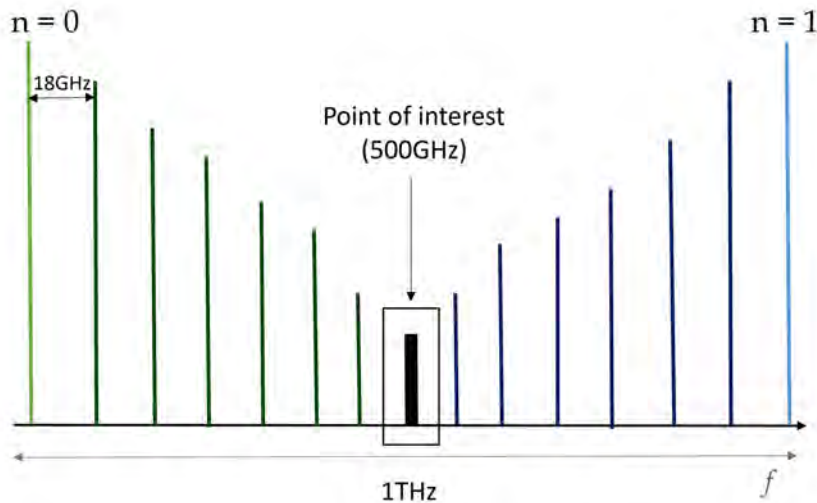


FIG. 12: Illustration of the two modes delineated in Figure 11, showcasing the ongoing creation of sidebands until reaching a frequency point of 500 GHz, the midpoint. It is essential to acknowledge that sidebands will persist in the same direction as their generation until they dissipate amidst the noise inherent to the Optical Spectrum Analyzer (OSA), making them irrelevant for the experiment's purposes.

**MI microcomb:** Another important aspect is the use of a mid-infrared (MI) microcomb, where two modes are selected to study the  $f_{rep}$ . Figure 13 shows an MI comb obtained before performing the EOM. A closer examination provided in figure 14 facilitates comprehension of the nature of the measurement being conducted.

MI microcombs demonstrate exceptional stability and reproducibility in the arrangement of comb lines (modes). Its creation involves detuning the laser from its original wavelength to a juncture where the FWM surpasses a predefined threshold power. Once initiated, a constant control over the regime of OFCs generation is imperative until achieving a state akin to that depicted in figure 13. The observation of multiple modes during the initial stages of OFC creation underscores the dynamic nature of the process, as it will be varying in spectrum and stability as the desired state is reached. In this state, numerous modes with equidistant frequencies and substantial power levels are observable [16].

In summary, throughout the process of creating OFCs, numerous modes emerge as the pump light enters the resonator. However, achieving the desired state necessitates a fixed power magnitude to be maintained consistently, and the properties of the resonator such as the index of refraction changes over time as nonlinear effects like Kerr effect or thermal non-stabilities arise in the state of comb creation.

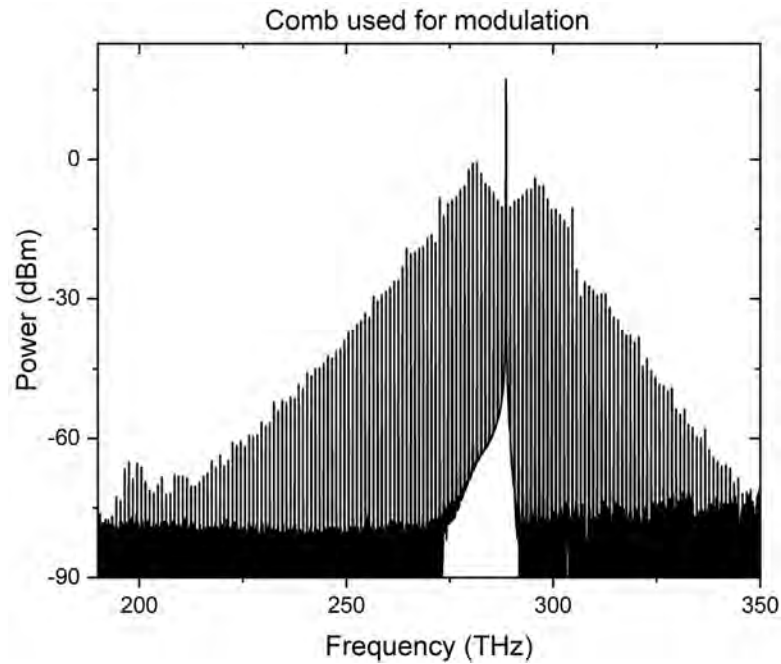


FIG. 13: Image of a MI comb created in the laboratory at a wavelength of 1039.660 nm. The creation of an MI comb necessitates precise control over laser detuning, ensuring meticulous adjustments in frequency to enter the resonance regime where FWM initiates the generation of comb modes.

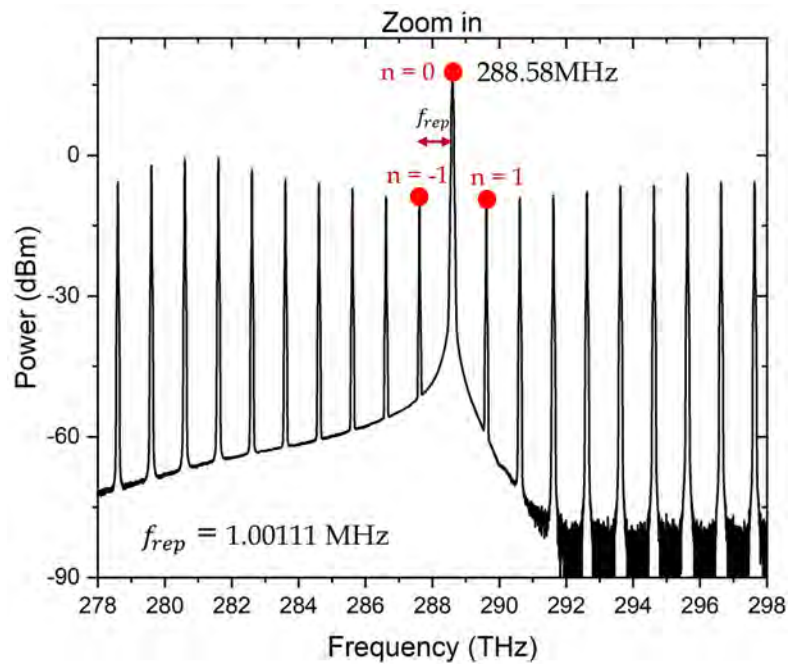


FIG. 14: Zooming into Figure 13, which depicts the MI comb, we observe the modes designated for modulation. Specifically, three of the  $n$ 's will undergo modulation, as the filter we utilize will isolate these two modes. This approach facilitates comparison between the different modulations across each branch of the modulation process. The  $f_{rep}$  is analyzed by conducting peak searches of the modes and averaging the differences between each, providing us with a rough estimation.

### 3. EXPERIMENTAL SET-UP

#### A. Description of the Experimental Configuration

**Radio Frequency part:** As illustrated in Figure 15, our experimental setup incorporates a Radio Frequency (RF) synthesizer, tasked with supplying the modulators with an 18 GHz  $f_m$  and the requisite  $V_{PP}$ . The RF synthesizer boasts the capability to generate a broad spectrum of frequencies from a single source, ensuring a stable 18 GHz  $f_m$  for the sidebands creation. Subsequently, the RF signal originated from the synthesizer is directed to each of the three distinct modulators responsible for generating the sidebands. One end remains grounded, as only three Electro-Optic Modulators (EOMs) are necessary to fulfill the experimental objectives. Following this, phase shifters are employed to fine-tune the phase of each electrical field affecting the respective modulator. This adjustment is crucial as it ensures the creation of modulated sidebands with optimal coherence between each generated sideband. Given that the sidebands overlap over time, the phase shifters play a vital role in maximizing constructive interference while minimizing destructive interference.

Additionally, 50/50 splitters are integrated into the setup to distribute  $f_m$  evenly to each of the modulators. This ensures uniform modulation across all modulators, contributing to the coherence and efficacy of the experimental setup.

**Optical Part:** In this Electro-Optic Modulator experiment, depicted in figure 16, the RF segment amplifies the RF signal from the synthesizer by 30 dBm to attain the required  $V_{PP}$  necessary for modulation. The Optical segment commences with the primary pump laser emitting 1  $\mu\text{m}$  optical light, which is directed into the microresonator to initiate the generation of the Mid-Infrared (MI) microcomb in pulse form. Subsequently, to focus solely on two modes within the microcomb spectrum, an optical bandpass filter with a bandwidth of  $\pm 5$  nm is employed, given the approximate 1 THz separation between modes.

Following the filtering, the resultant two modes are amplified using a Booster Optical Amplifier (BOA) to regulate the input of comb light into the modulators. Considering that the modulators, as per Eqn. 2, attenuate the signal amplitude, it is imperative to amplify the signal to prevent it from diminishing below -40 dBm (0.1  $\mu\text{W}$ ), a level comparable to noise in the OSA. Finally, the light proceeds to the modulation stage, where sidebands are generated. An OSA is utilized for spectrum analysis, capable of recording frequencies from Hz to THz. Notably, due to limitations in accurately capturing data points beyond the THz range, the OSA is particularly employed for studying the 18 GHz modulation frequency, well-suited for this frequency analyzer. Additionally, for enhanced resolution in the analysis of lower frequencies such as MHz or kHz, a photodetector with superior resolution is integrated as needed. Figures 17 and 18 show an image of the filter and the optical table, respectively, where all components were assembled and calibrated.

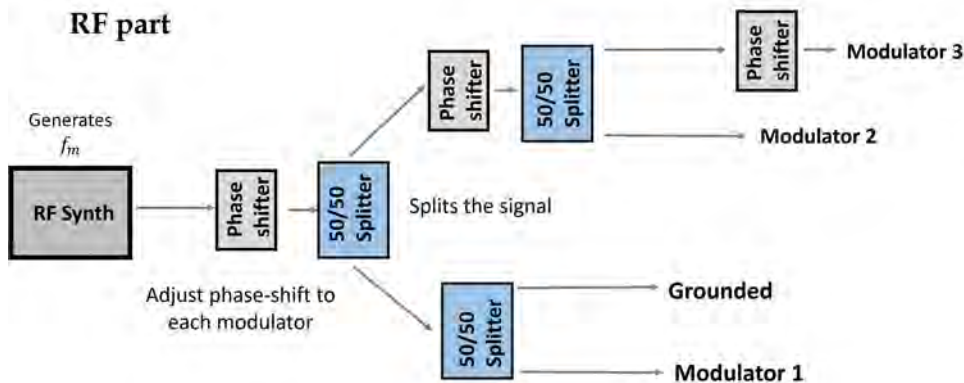


FIG. 15: Illustration of the Radio Frequency setup, showcasing the utilization of three modulators. For each modulator, three phase shifters are employed to regulate the phase of the respective electric field generated for each sideband. The signal is split to enable independent control of each modulator, ensuring consistent modulation with the  $V_{PP}$  and  $V_{\pi}$ .

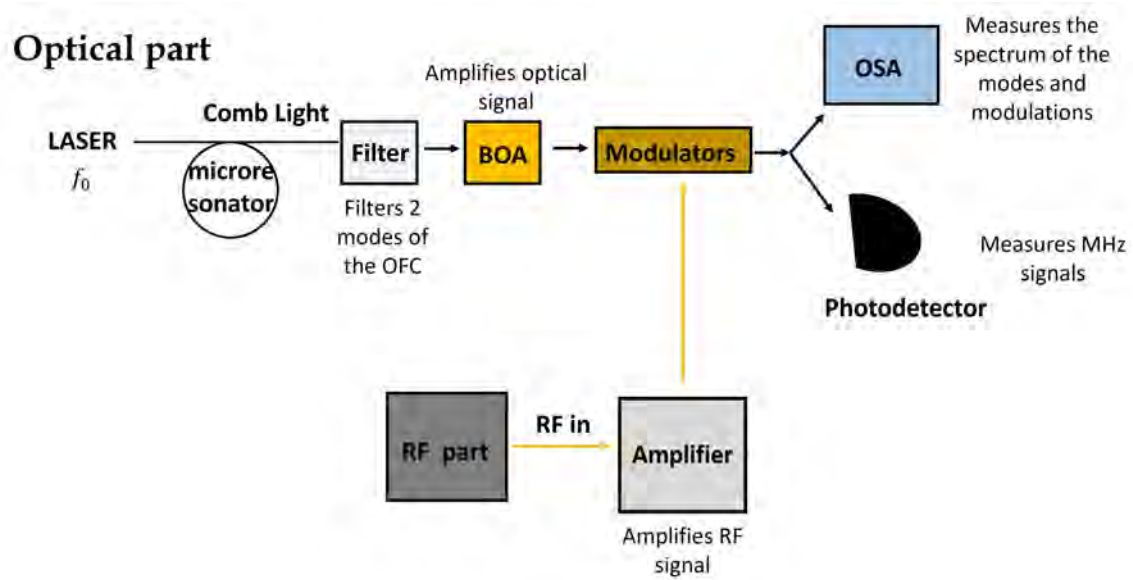


FIG. 16: Illustration of optical setup. Initially, the generated comb light is filtered to isolate two specific modes. Subsequently, these modes are amplified using a Boost Optical Amplifier to compensate for losses incurred during microcomb creation and filtering. Following amplification, the modes are modulated, resulting in the production of sidebands. These sidebands are then analyzed using either an OSA or a photodetector, depending on the specific objectives of the measurement.

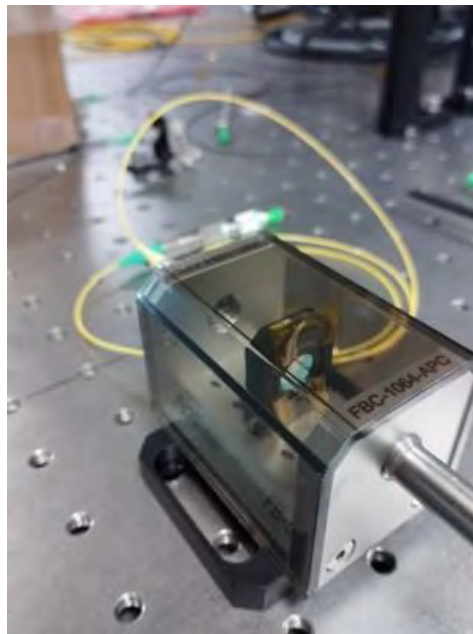


FIG. 17: Real image of the filter, in this case is a free space bandpass filter for ranges of  $1040\text{nm} \pm 5 \text{ nm}$ . It is implemented through an U-Bench.

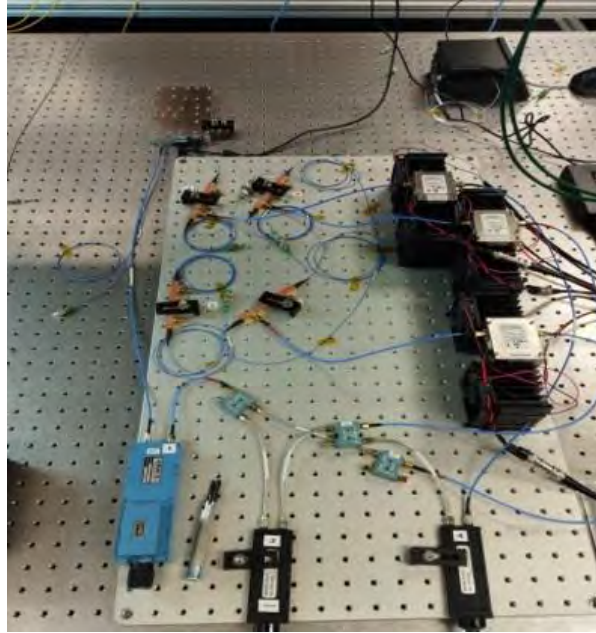


FIG. 18: This is a photograph of the setup. The orange prisms are the modulators, although there are four available, only three are utilized. The large silver box is identified as the synthesizer, while the blue and two black devices positioned at the bottom are the phase shifters. Additionally, the small blue square-shaped apparatus serves as the splitters. Furthermore, the black boxes situated on the right side are the RF amplifiers, and the one positioned in the right corner is designated as the Booster Optical Amplifier (BOA).

## B. Calibration and Control Procedure

**Phase shifters:** Among the components comprising this experiment, the phase shifters hold particular significance. As depicted in figures 19 and 20, precise adjustment of the phase for each modulator is essential to achieve optimal modulation, ensuring the proper superposition of the electric fields from each sideband. This optimization allows for accurate determination and adjustment of prominent peaks within the frequency spectrum, ensuring they exhibit distinct peaks rather than flat lines, thereby facilitating comprehensive analysis.

The adjustment process involves manual adjusting of the knobs of each phase shifter, iteratively optimizing their alignment to ensure constructive interference and clear peak visibility in the modulation direction. This visual assessment through the OSA is crucial for maximizing modulation effectiveness and achieving desired spectral features. Figure 19 illustrates the creation of sidebands; however, some may exhibit less pronounced peaks compared to figure 20, where sidebands appear more distinct. Additionally, the seemingly flat profile in the middle of figure 20 corresponds to the main laser pump, a consistent feature expected in the spectrum, that can vary but does not affect the experiment.

**RF Synthesizer:** This is one of the most important component of the set-up as it regulates the  $V_{PP}$  applied to the EOMs. Additionally, it is imperative to account for the considerable losses incurred across the Radio Frequency (RF) segment. Despite the mitigation of losses, such as those occurring between the phase shifters and the beamsplitter, some of them remains inevitable. Hence, it became imperative to quantify the power entering the modulators using a Spectrum Analyzer (ESA) post-amplification. A critical consideration was the 35 dBm power amplification output from the amplifiers to each modulator. Following the measurement of losses across all components, it was determined that inputting 10 dBm from the synthesizer would approximately yield the necessary 30 dBm (1 W) at each modulator. This power level was deemed sufficient to drive each modulator to the requisite modulation depth required to span 1 THz adequately. However, the characterization process was constrained by the ESA's inability to measure signals exceeding 30 dBm. To overcome this limitation, testing was conducted using the OSA when approaching the upper limit, ensuring comprehensive assessment of the required power to complete the spectral span necessary for achieving the modulation depth showed previously.

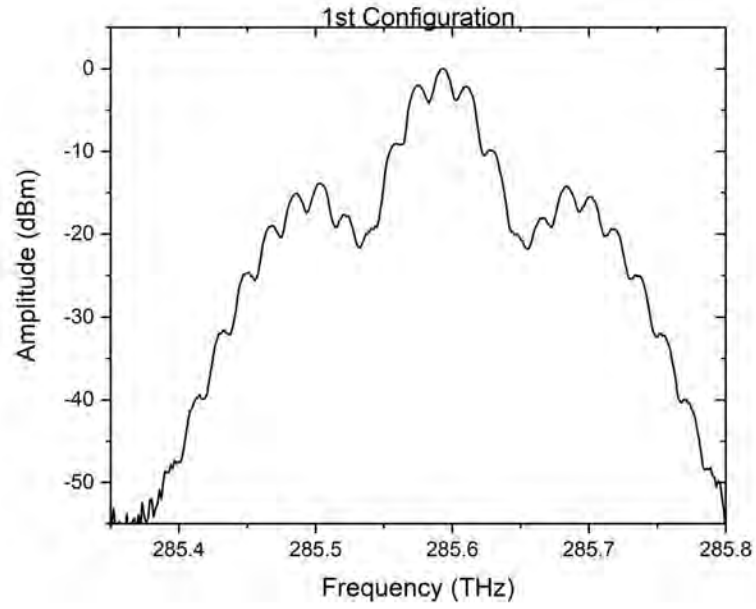


FIG. 19: Frequency spectrum of a single mode after modulation, with no phase-shift adjustment, exhibits areas where peaks suggestive of sidebands should be apparent. However, the presence of discernible sidebands is ambiguous in certain regions, as some portions of the spectrum appear either flat or indistinct, rendering it unclear whether sidebands are present or not.

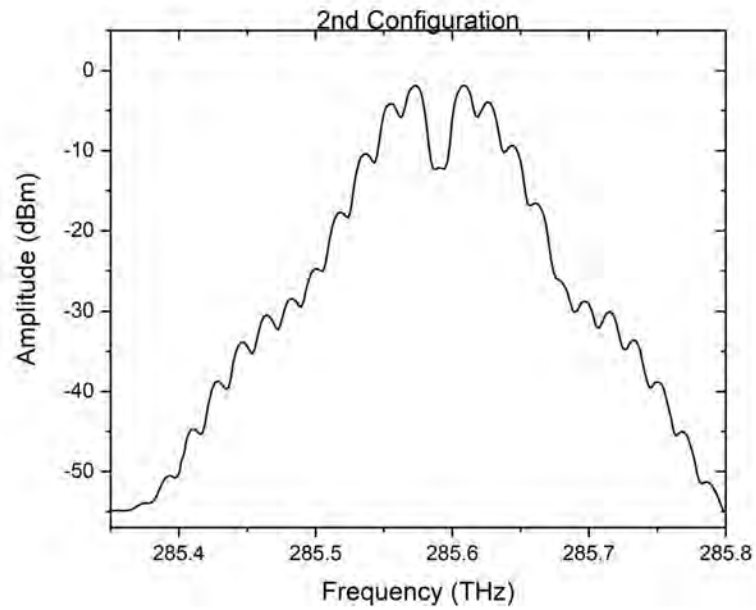


FIG. 20: Frequency spectrum of a single mode after modulation, with a phase-shift adjustment, demonstrates improved clarity of the sidebands. In contrast to Figure 19, the sidebands are more distinct and exist within a regime of higher power. This indicates that the sidebands are not only discernible but also measurable, with power levels above -40 dBm, leading to a meaningful result.

## 4. RESULTS

### A.Measured EOM microcomb

The initial outcome of this EOM experiment involved demonstrating the behavior of an array of EO modulators by achieving full spanning from a single mode utilizing the entire modulation capability of the setup. Figure 21 illustrates the resultant modulation, wherein most of the sidebands generated overlap, effectively developing a complete 1 THz modulation spectrum with well-defined peaks. With an input power of 10 dBm and an average power of approximately 29 dBm into each modulator, a total of 66 sidebands per side, with power levels higher than -40 dBm, were observed, spanning roughly 18 GHz each.

Following this demonstration, the experiment progressed to inputting two modes, as depicted in figure 22. Here, the desired modulation pattern is evident, featuring the main mode at 288.356 THz and the accompanying sidebands spanning the entire frequency repetition range of the mode. Through adjustment of the phase shifters and input power, the 66 sidebands per side for the 1 THz spanning were successfully obtained, achieving full modulation depth. Furthermore, the adjacent modes of the MI comb, notably at  $n = -1$  (287.353 THz) and  $n = 1$  (289.287 THz), each spanning approximately 1 THz, were identified. These modes were selected by iteratively adjusting the phase shifters and input power to optimize sideband emergence and disappearance. The generation of power was observed to peak when the RF synthesizer power reached 11 dBm, beyond which no additional modulation was discernible.

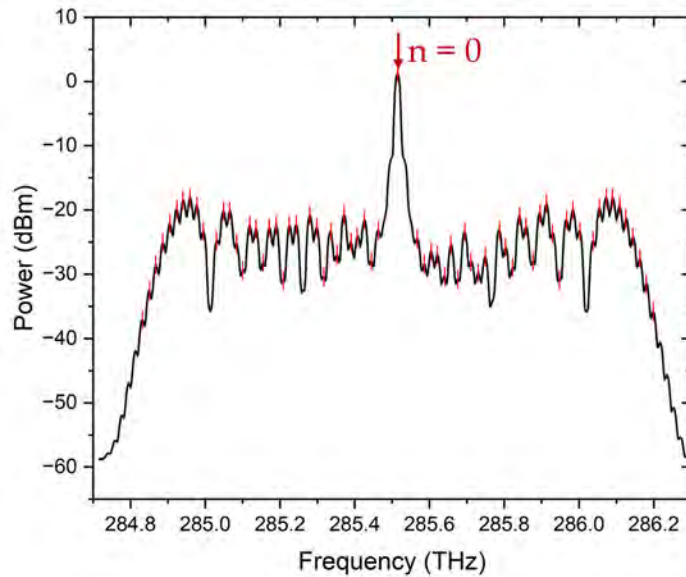


FIG. 21: . The EO modulation initiated from the main laser  $n=0$ , centered at 285.523 THz, results in sidebands expanding both to the left and right. These sidebands extend to more than 0.5 THz, indicating that the modulators possess the capability to generate an ample number of sidebands to span the required frequency range. Optimized peaks of the sidebands are highlighted with red lines, emphasizing their significance in the modulation process.

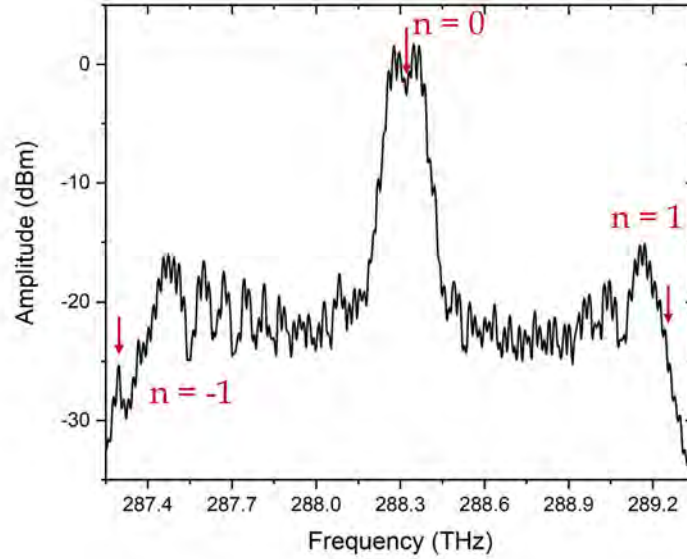


FIG. 22: Results from the EO modulation, where it is initiated from the main laser, centered at 288.356 THz ( $n = 0$ ). Subsequent to modulation, the next two modes filtered are observed at 287.353 THz ( $n = -1$ ) and 289.287 THz ( $n = 1$ ). This illustrates the full modulation required to achieve the objectives of the experiment and hence the complete spanning of 1 THz with the sidebands generated through the EOM, showcasing the capability to manipulate the modulation and subsequently study the complete EOM setup and the  $f_{rep}$  of our device.

### B. Suggestions for Further Research and Development

As mentioned previously, a photodetector was utilized to detect signals in the MHz or kHz range. This was necessary because, as depicted in figure 23, at the midpoint of the  $f_{rep}$ , where the two modulations from the two modes converge, there exists a point where two sidebands either overlap or are in close proximity, rendering them difficult to measure accurately with the OSA. This occurs due to imperfections and fluctuations in the modulation process, resulting in incomplete separation of the sidebands by the specified 18 GHz frequency spacing. Despite this challenge, this two close sidebands, known as the beatnote, can still be resolved and measured using a photodetector. The formula for calculating the beatnote is as follows:

$$f_{beat} = |(m + n) * f_m - f_{rep}|. \quad (5)$$

Where  $m$  and  $n$  are the number of sidebands created in each direction. This elucidates that once the number of achievable sidebands is determined, it becomes feasible to set  $f_{beat}$  to any value other than 0, since  $f_m$  and  $f_{rep}$  should remain constant. Thereby making  $f_{beat}$  measurable within the range of the photodetector. However, measuring this beatnote presents a complex challenge due to the previously mentioned fluctuations in the modulation process, necessitating enhanced control over the modulation to resolve and observe it accurately. Despite theoretical calculations indicating that at a modulation frequency of  $f_m = 17.858$  GHz, a 100 MHz beatnote should be observable, practical experimentation failed to confirm this. Instead, various frequencies were observed, none of which precisely matched the expected signal. Furthermore, these frequencies exhibited variability over time due to fluctuations in the  $V_{PP}$ , which was constantly changing. Enhanced control over the RF signal, addressing the inherent challenges associated with RF devices, is imperative to accurately determine the beatnote signal and subsequently achieve the optimal  $f_{rep}$  for our microcombs.

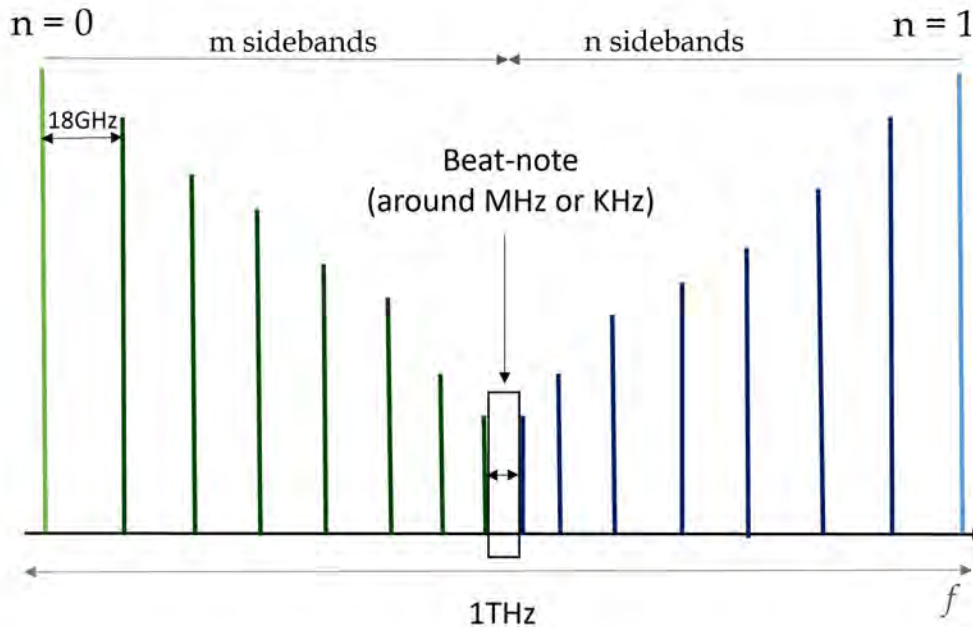


FIG. 23: Illustration of the beatnote originated in the midpoint where the sidebands of each side converge. This point of interest can be determined by Eqn 5. once the EOM is fully developed in the modes, and therefore the number of sidebands are known based on the  $f_m$  needed to get any  $f_{beat}$ .

### C. Conclusion

In this experiment, we successfully achieved an EOM of 1 THz. This capability to modulate light at such high frequencies opens up numerous possibilities across various fields including photonics, telecommunications, and spectroscopy. Our findings demonstrate an approach to measuring the frequency of repetition, diverging from conventional methods and potentially offering a more precise definition of the limits microcomb generation and behaviour. However, despite achieving the desired modulation, the inability to observe the beatnote warrants further investigation. The absence of the beatnote, typically arising from interference between two modulated and overlapped sidebands, suggests potential challenges within our RF and optical setup. Enhancing the control over RF signal properties and its fluctuations, such as an exact frequency of modulation and phase, without variation could potentially improve modulation depth and enhance beatnote visibility. Additionally, further investigation into inefficiencies of the EO modulators, such as thermal bistabilities affecting the properties of the  $\text{LiNbO}_3$  material, may prove beneficial. In conclusion, while further investigation is necessary to fully uncover the beatnote in our devices, our results highlight the immense potential of electro-optic modulation at high frequencies. Through continued experimentation, we aim to precisely determine the exact  $f_{rep}$  of microring resonator devices, leading to a deeper understanding of their limitations and facilitating tailored design for various applications.

### ACKNOWLEDGEMENTS

I would like to thank my colleague, the PhD student Gabriel Colacion for his guidance and support throughout this project, specially when building and characterizing the set-up. I would also like to thank my advisor Dr. Drake for her insight, support and providing the devices and tools in the laboratory 165 in the Center for High Technology Materials at University of New Mexico. Finally, I would like to express my gratitude to the Rayburn Reaching Up Fund for providing funding for this project.

- 
- [1] N. Picqué and T. W. Hänsch, “Frequency comb spectroscopy,” *Nature Photonics* **13**, 146-157 (2019).
  - [2] T. J. Kippenberg, R. Holzwarth and S. A. Diddams, ”Microresonator-Based Optical Frequency Combs,” *Science* **332** , 555-559 (2011).
  - [3] T. J. Kippenberg, R. Holzwarth, S. A. Diddams, ”Microresonator-based optical frequency combs,” *Science* **29**;332(6029):555-9 (2011).
  - [4] H. Jung, *et al.*, ”Optical frequency comb generation from aluminum nitride microring resonator,” *Opt. Lett.* **38**, 2810-2813 (2013).
  - [5] D. T. Spencer, *et al.*, ”An optical-frequency synthesizer using integrated photonics,” *Nature* **557**, 81–85 (2018).
  - [6] V. Brasch, *et al.*, ”Radiation hardness of high-Q silicon nitride microresonators for space compatible integrated optics,” *Opt. Express* **22**, 30786-30794 (2014).
  - [7] K. J. Vahala, ”Optical microcavities,” *Nature* **424**, 839–846 (2003). (with M. Cai)
  - [8] S. B. Papp, P. Del’Haye, S.A. Diddams, ”Mechanical Control of a Microrod-Resonator Optical Frequency Comb,” *Phys. Rev.* **X3**, 031003 (2013).
  - [9] Q. Li, M. Davanço, K. Srinivasan, ”Efficient and low-noise single-photon-level frequency conversion interfaces using silicon nanophotonics,” *Nature Photon* **10**,406–414 (2016).
  - [10] T. J. Kippenberg, ”Nonlinear Optics in Ultra-High-Q Whispering-Gallery Optical Microcavities,” Dissertation (Ph.D.), California Institute of Technology. Jan August (2004).
  - [11] H. Lee, T. Chen, J. Li, *et al.*, ”Chemically etched ultrahigh-Q wedge-resonator on a silicon chip,” *Nature Photon* **6**, 369–373 (2012).
  - [12] Tobias J. Kippenberg, *et al.* Dissipative Kerr solitons in optical microresonators. *Science* **361**, eaan8083(2018)
  - [13] R. Paschotta, article on Pockels effect in the *Encyclopedia of Laser Physics and Technology*, **1** . edition October 2008, Wiley-VCH, ISBN 978-3-527-40828-3
  - [14] Practical Uses and Applications of Electro-Optic Modulators from Newport webpage.
  - [15] Proposed Approach for Driving EO Phase Modulators from Thorlabs webpage.
  - [16] Alessia Pasquazi, Marco Peccianti, *et al.*, ”Micro-combs: A novel generation of optical sources”, *Physics Reports* **729** (2018).